Research Article

Ireneusz Wlodarczyk*, Kazimieras Černis, and Ilgmar Eglitis

Asteroids discovered in the Baldone Observatory between 2017 and 2022: The orbits of asteroid 428694 Saule and 330836 Orius

https://doi.org/10.1515/astro-2024-0004
received January 31, 2023; accepted June 07, 2024

Abstract: We discovered 83 asteroids at the Baldone Astrophysical Observatory (MPC code 069) in 2017–2022. We studied one of the dynamically interesting Apollo (Near Earth object) observed at the Baldone Astronomical Observatory, namely 428694 Saule (2008 OS9) and the Centaur-type asteroid 330836 Orius (2009 HW77). We studied the evolution of the asteroid Saule's rotation period, obliquity, and spin axis together with its non-gravitational parameter da/dt connected with the Yarkovsky effect. Additionally, we studied the orbit of the Amor-type asteroid 2017 UW42, which has the significant non-gravitational parameter $A2$.

Keywords: minor planets, asteroids, search, astrometry, orbits

Acronyms

CA	Close approach
IAU MPC	International Astronomical Union Minor Planet Center
LOV	Line of variation; LOV is a one-dimensional part of a (curved) line in the initial conditions space generally computed with the uniform sampling of the LOV parameter
MPC	Minor planet center
MPEC	Minor Planet electronic circulars
NEO	Near Earth object
NEODyS	Near Earth objects dynamical site
NEODyS-2	Near Earth objects dynamic Site-2
YORP effect	The Yarkovsky–O'Keefe–Radzievskii–Paddack effect
σLOV	denotes the position along the line of variation (LOV), in the σ space
σ	Values of σ are usually in the interval (−3, 3)
RMSast	root mean square error (of the residuals O–C) of the orbital fit
RMSmag	root mean square error of observation's magnitude
VA	Virtual asteroid, clones
Symbols:	
H	absolute magnitude of an asteroid
pV	albedo
ϱ	density

1 Introduction

In Cernis *et al.*, (2015) and Wlodarczyk *et al.*, (2020), we presented the discovered asteroids at the Baldone Observatory (located in Latvia) from 2008–2018. In the present work, we gather all discoveries of asteroids from 2017 through 2022. The work continues our discoveries and attempts to discover new asteroids. The discovery of any new object is valuable for science. There may be ordinary objects between them, especially a Near Earth object (NEO). Moreover, with standard observations, it is possible

*** Corresponding author: Ireneusz Wlodarczyk,** Chorzow Astronomical Observatory, 41-500 Chorzow, Poland, e-mail: astrobit@ka.onet.pl
Kazimieras Černis: Institute of Theoretical Physics and Astronomy, Vilnius University, Saulėtekio al. 3, Vilnius LT-10222, Lithuania, e-mail: Kazimieras.Cernis@tfai.vu.lt
Ilgmar Eglitis: Institute of Astronomy, University of Latvia, Raina 19, Riga 1586, Latvia, e-mail: ilgmars@latnet.lv

to find unique comets with hyperbolic orbits that may come to us from another star system.

All orbital computations of asteroids are made using the OrbFit software v.5.0.5 and v.5.0.6. In the last version, the NEODyS Team introduced the error weighing model described by Veres *et al.*, (2017), as announced by F. Bernardi on the Minor Planet Mailing List. We used the JPL DE431 Ephemerides with 17 perturbing massive asteroids as was described in Farnocchia *et al.*, (2013a,b) and similar to Wlodarczyk (2015).

2 Discoveries of minor planets at the Baldone Observatory in 2017–2022

Table 1 lists 83 asteroids discovered at the Baldone Astrophysical Observatory in Latvia, and Table 2 presents statistics and astrometric observations of the asteroids (both new and known) at the Baldone Observatory in 2017–2022.

In 2015–2017, only some orbits of objects were calculated because there needed to be complete information. The orbits of the following asteroids are computed with low accuracy because of their short observational arc: 2017 SR313, 2018 GE3, and 2019 SJ173.

This work presents the full set of discovered objects in 2017–2022. All discoveries and observations of asteroids at Baldone were made by K. Cernis (KC) and I. Eglitis (IE).

In Wlodarczyk *et al.*, (2020), 37 asteroids were discovered in 2015–2018. In Wlodarczyk *et al.*, (2020), in 2017, 21 objects were discovered; in the present paper (2023), there are 54 objects because the MPC has credited us with additional 33 discoveries in the last 3 years. In Wlodarczyk *et al.*, (2022a) in 2018, 9 objects were discovered and 14 in the new paper (2023) because the Minor planet center (MPC) has made five additional discoveries in the last 3 years. At the same time, in the last 3 years, there have been a lot of new sightings of the objects mentioned in Wlodarczyk *et al.*, (2020). We decided to show all objects from Wlodarczyk *et al.*, (2020) and additional discoveries in 2017–2018. We have given references to each object's MPC and MPO numbers, and MPC has given us new designations. Moreover, the number of published astrometric observations remained the same as in Wlodarczyk *et al.*, (2020). We should have mentioned that the numbers in Table 2 refer to Minor Planet Circular numbers.

Recently, Quenzi Ye from the University of Maryland, USA, compiled an interesting statistic of asteroid discoveries: https://sbnmpc.astro.umd.edu/mpecwatch/obs.html. According to Quenzi, the designations in his list are as follows: F/U – follow-up;1st F/U – first to follow-up; Prec. – precovery. In detail, "First follow-up" means being the first to confirm an object. For example, here in https://minorplanetcenter.net/mpec/K22/K22WS5.html, G96 is the discoverer, and L01 was the first to follow up.

For now, this service only analyzes observations/discoveries announced by Minor Planet electronic circulars (NEOs, comets). Quenzi might include main belters in the future. Shortly, the discoveries of the asteroids from Baldone should also be included there.

3 Orbital and physical evolution of the asteroid 428694 Saule (2008 OS9)

KC and IE discovered asteroid 428694 Saule (2008 OS9) at Baldone on 2008-07-29. The orbit type of this asteroid is Apollo and Near Earth Asteroid. Asteroid 428694 Saule (2008 OS9) is named after Saule, a solar goddess, the solar deity in the Latvian and Lithuanian mythologies (MPC 10061).

3.1 Starting orbital elements

To compute starting orbital elements of the asteroid Saule, we used the OrbFit software with the JPL DE431 ephemerides, weighting and selecting observations according to the NEODyS-2[1], 17 additional massive asteroids, and the Yarkovsky effects. We searched for the non-gravitational parameter $A2$, computed directly from observations. $A2$ is a non-gravitational transverse acceleration parameter. We used the publicly available OrbFit v.5.0.5 and 5.0.7 software[2]. These versions can compute orbits using dynamical parameters connected to the non-gravitational perturbations. We calculated the non-gravitational parameter $A2$. We used all 593 observations published by the IAU MPC: https://minorplanetcenter.net/db_search, from 2008 07 25.36573 to 2022 08 19.308671.

According to the OrbFit v.5.0.7, we used the error model *vfcc17* of Veres *et al.*, (2017). Table 3 presents the starting nominal Keplerian orbital elements of the 428694

1 https://newton.spacedys.com/neodys/
2 https://newton.spacedys.com/neodys/

Table 1: List of asteroids discovered at the Baldone Observatory in 2017–2022

No.	Date of discovery	Designation	Number	Status	MPC reference
1	2017 Sep. 25	2017 SV33		ID 4 op.	MPC 106,573 (2017 Nov. 5)
2	2017 Sep. 25	2017 SW33	512,962	ID 9 op.	MPC 106,573 (2017 Nov. 5)
3	2017 Sep. 26	2017 SX33		ID 7 op.	MPC 106,573 (2017 Nov. 5)
4	2017 Sep. 28	2017 SY33	506,714	ID 9 op.	MPC 106,573 (2017 Nov. 5)
5	2017 Sep. 26	2017 SO42		*3 op.	MPC 106,573 (2017 Nov. 5)
6	2017 Sep. 29	2017 SK134		*6 op.	MPC 118,948 (2020 Jan. 9)
7	2017 Sep. 26	2017 SP136		*60-day arc	MPC 118,948 (2020 Jan. 9)
8	2017 Sep. 25	2017 SY166		*40-day arc	MPC 118,948 (2020 Jan. 9)
9	2017 Sep. 26	2017 SR169		ID 5 op.	MPC 118,948 (2020 Jan. 9)
10	2017 Sep. 27	2017 SK170		ID 45-day arc	MPC 118,948 (2020 Jan. 9)
11	2017 Sep. 26	2017 SM172		ID 6 op.	MPC 118,948 (2020 Jan. 9)
12	2017 Sep. 26	2017 SF175		ID 4 op.	MPC 118,948 (2020 Jan. 9)
13	2017 Sep. 29	2017 SX187		*45-day arc	MPC 118,948 (2020 Jan. 9)
14	2017 Sep. 25	2017 SO205		ID 6 op.	MPC 123,568 (2020 Aug. 7)
15	2017 Sep. 29	2017 SK220		ID 4 op.	MPC 125,601 (2020 Nov. 17)
16	2017 Sep. 29	2017 SH213		ID 4 op.	MPC 124,649 (2020 Sep. 24)
17	2017 Sep. 26	2017 SQ228		*3 op.	MPC 129,111 (2021 Mar. 25)
18	2017 Sep. 29	2017 SM265		*2 op.	MPC 134,098 (2021 Sep. 20)
19	2017 Sep. 27	2017 SA275		*3 op.	MPC 134,098 (2021 Sep. 20)
20	2017 Sep. 25	2017 SR313		*26-day arc	MPC 141,310 (2022 Jul. 19)
21	2017 Oct. 18	2017 UT9		ID 3 op.	MPC 106,573 (2017 Nov. 5)
22	2017 Oct. 18	2017 UU9	585,101	ID 7 op.	MPC 106,573 (2017 Nov. 5)
23	2017 Oct. 19	2017 UO11	585,107	ID 8 op.	MPC 106,573 (2017 Nov. 5)
24	2017 Oct. 19	2017 UP11	50,7546	ID 11 op.	MPC 106,573 (2017 Nov. 5)
25	2017 Oct. 19	2017 UQ11		ID 3 op.	MPC 106,573 (2017 Nov. 5)
26	2017 Oct. 19	2017 UR11	585,108	ID 7 op.	MPC 106,573 (2017 Nov. 5)
27	2017 Oct. 19	2017 US11	508,671	ID 8 op.	MPC 106,573 (2017 Nov. 5)
28	2017 Oct. 19	2017 UT11		ID 4 op.	MPC 106,573 (2017 Nov. 5)
29	2017 Oct. 19	2017 UU11	540,601	ID 11 op.	MPC 106,573 (2017 Nov. 5)
30	2017 Oct. 19	2017 UV11		ID 8 op.	MPC 106,573 (2017 Nov. 5)
31	2017 Oct. 21	2017 UV125		*4 op.	MPC 129,111 (202 Mar. 25)
32	2017 Oct. 19	2017 UW11	508,672	ID 12 op.	MPC 106,573 (2017 Nov. 5)
33	2017 Oct. 19	2017 UX11	540,602	ID 8 op.	MPC 106,573 (2017 Nov. 5)
34	2017 Oct. 19	2017 UY11		ID 5 op.	MPC 106,573 (2017 Nov. 5)
35	2017 Oct. 22	2017 UJ15	545,611	ID 11 op.	MPC 106,573 (2017 Nov. 5)
36	2017 Oct. 22	2017 UK15		ID 6 op.	MPC 106,573 (2017 Nov. 5)
37	2017 Oct. 22	2017 UL15		ID 5 op.	MPC 106,573 (2017 Nov. 5)
38	2017 Oct. 19	2017 UT56		*80-day arc	MPC 118,948 (2020 Jan. 9)
39	2017 Oct. 19	2017 UU58		ID 4 op.	MPC 118,948 (2020 Jan. 9)
40	2017 Oct. 18	2017 UB63		ID 3 op.	MPC 118,948 (2020 Jan. 9)
41	2017 Oct. 23	2017 UR64		*4 op.	MPC 118,948 (2020 Jan. 9)
42	2017 Oct. 19	2017 UV64		ID 2 op.	MPC 118,948 (2020 Jan. 9)
43	2017 Oct. 19	2017 UY64		ID 4 op.	MPC 118,948 (2020 Jan. 9)
44	2017 Oct. 19	2017 UX71		ID 6 op.	MPC 118,948 (2020 Jan. 9)
45	2017 Oct. 21	2017 UB76		ID 6 op.	MPC 118,948 (2020 Jan. 9)
46	2017 Oct. 19	2017 UK78		*40-day arc	MPC 118,948 (2020 Jan. 9)
47	2017 Oct. 19	2017 UM95		*6 op.	MPC 123,568 (2020 Aug. 7)
48	2017 Oct. 23	2017 UX95		*7 op.	MPC 123,568 (2020 Aug. 7)
49	2017 Oct. 23	2017 UK101		*6 op.	MPC 123,568 (2020 Aug. 7)
50	2017 Oct. 21	2017 UM164		*3 op.	MPC 135,342 (2021 Oct. 27)
51	2017 Oct. 23	2002 AN214	567,580	N9 op.	MPO 995 (2023 Jan. 23)
52	2017 Nov. 17	2017 WT35		ID 4 op.	MPC 118,948 (2020 Jan. 9)
53	2017 Nov. 17	2017 WW49		*5 op.	MPC 125,601 (2020 Nov. 17)
54	2017 Nov. 16	2017 WG88		*2 op.	MPC 141,310 (2022 Jul. 19)
55	2018 Mar. 18	2018 FU25		ID 14 op.	MPC 109,684 (2018 Apr. 30)
56	2018 Mar. 18	2018 FV25		ID 11 op.	MPC 109,684 (2018 Apr. 30)

(Continued)

Table 1: *Continued*

No.	Date of discovery	Designation	Number	Status	MPC reference
57	2018 Mar. 16	2018 FL30		*35-day arc	MPC 118,948 (2020 Jan. 9)
58	2018 Apr. 13	2018 GE3	NEO object	ID 4-day arc	MPO 445,234 (2018 Apr. 30)
59	2018 Apr. 10	2018 GU6		ID 8 op.	MPC 109,684 (2018 Apr. 30)
60	2018 Apr. 10	2018 GV6	585,398	ID 6 op.	MPC 109,684 (2018 Apr. 30)
61	2018 Apr. 12	2018 GX8		ID 2 op.	MPC 109,684 (2018 Apr. 30)
62	2018 Apr. 10	2018 GV15		*5 op.	MPC 123,568 (2020 Aug. 7)
63	2018 Sep. 10	2018 RG17		*5 op.	MPC 110,809 (2018 Sep. 25)
64	2018 Sep. 10	2018 RH17	542,935	ID 8 op.	MPC 110,809 (2018 Sep. 25)
65	2018 Sep. 13	2018 RW41		*4 op.	MPC 118,948 (2020 Jan. 9)
66	2018 Oct. 6	2018 TL9		ID 9 op.	MPC 112,836 (2019 May. 18)
67	2018 Oct. 6	2018 TM9		*2 op.	MPC 112,836 (2019 May. 18)
68	2018 Oct. 7	2018 TF19	560,161	ID 8 op.	MPC 118,948 (2020 Jan. 9)
69	2019 Mar. 31	2019 FU4	603,184	ID 8 op.	MPC 112,836 (2019 May. 18)
70	2019 Apr. 1	2019 GJ8	573,235	ID 6 op.	MPC 112,836 (2019 May. 18)
71	2019 Apr. 1	2019 GK8	603,397	ID 9 op.	MPC 112,836 (2019 May. 18)
72	2019 Apr. 1	2019 GL8		ID 2 op.	MPC 112,836 (2019 May. 18)
73	2019 Apr. 1	2019 GM8		ID 7 op.	MPC 112,836 (2019 May. 18)
74	2019 Apr. 1	2019 GN8		ID 6 op.	MPC 112,836 (2019 May. 18)
75	2019 Apr. 1	2019 GO8		ID 9 op.	MPC 112,836 (2019 May. 18)
76	2019 Mar. 26	2019 FQ8		*2 op.	MPC 118,948 (2020 Jan. 9)
77	2019 Sep. 22	2019 SN19	599,705	ID 4 op.	MPC 118,948 (2020 Jan. 9)
78	2019 Sep. 27	2019 SO29		*40-day arc	MPC 118,948 (2020 Jan. 9)
79	2019 Sep. 26	2019 SH61		*35-day arc	MPC 118,948 (2020 Jan. 9)
80	2019 Sep. 26	2019 SZ140		*40-day arc	MPC 129,111 (2021 Mar. 25)
81	2019 Sep. 26	2019 SJ173		*12-day arc	MPC 130,731 (2021 Jun. 1)
82	2019 Sep. 26	2019 SC183		*4 op.	MPC 134,098 (2021 Sep. 20)
83	2020 Aug. 11	2020 PC10		ID 42-day arc	MPC 125,601 (2020 Nov. 17)

Noted: Main-belt Asteroid 567,580 (2002 AN214) was named Latuni.
mark ID denotes independent discovery.
op. – opposition.
N – named asteroid.
mark * denotes that discoverer credit will be done for Baldone, when the object is numbered.

Saule (2008 OS9) asteroid computed using the mentioned OrbFit v.5.0.7 software.

It is worth noting that two other interesting recent methods of computations of the non-gravitational parameter $A2$ are in Perez-Hernandez and Benet (2022) and Dziadura *et al.*, (2022).

3.2 Starting physical parameters

Next, we used the mercury software of Fenucci and Novakovic (2022). As stated in https://github.com/Fenu24/mercury, this is a modified version of the N-body code mercury by Chambers (1999) (https://github.com/Fenu24/mercury/tree/master/doc), which includes the Yarkovsky and YORP effects for the dynamics of small solar system objects.

The Yarkovsky effect was discovered by the Polish-Russian civil engineer Ivan Osipovich Yarkovsky: https://en.wikipedia.org/wiki/Yarkovsky_effect.

We have a diurnal effect and a seasonal effect. Both effects produce a shift in the semimajor axis of the asteroid. The influence of the Yarkovsky effect on the motion of an object is evident over a long time, for example, in the motion of members of asteroid family *e.g.*, Novakovic *et al.*, (2022), Wlodarczyk and Leliwa-Kopystynski (2018), studying retrograde orbits in Wlodarczyk (2022b) or dangerous asteroids (Wlodarczyk 2020). To study the motion of asteroids and comets with the influence of the Yarkovsky effect, we use the non-gravitational parameters $A2$ and $\mathrm{d}a/\mathrm{d}t$. Both values of $A2$ and $\mathrm{d}a/\mathrm{d}t$ can be determined during orbit determination as a seventh parameter together with six other orbital parameters, *i.e.*, Keplerian elements. In Wlodarczyk (2018), several non-gravitational parameters A2 and $\mathrm{d}a/\mathrm{d}t$ were

Table 2: Statistics of asteroid discoveries and astrometric observations of the asteroids (both new and known) at the Baldone Observatory in 2017–2022

Year	Number of asteroid discoveries	Number of asteroid observations	Number of asteroids observed	MPC numbers
2017	54	3,798	972	102,359, 103,149, 104,117, 104,989, 105,343, 105,715, 106,573, 107,170
2018	14	5,561	1,516	107,827, 108,759, 109,228, 109,684, 110,175, 110,809, 111,864
2019	14	3,807	1,071	112,836, 115,067, 115,989, 117,290, 118,277
2020	1	3,135	863	118,948, 120,147, 121,322, 122,837, 123,568, 124,648, 125,601
2021	0	3,749	879	127,456, 129,111, 13,731, 132,404, 134,098, 135,342
2022	0	9,492	470	136,731, 138,608, 140,114, 141,310, 142,136, 158,705
Total	83	29,542	5,771	

computed. The advantage of the method used in the present work is that it simultaneously shows the evolution of P, gamma, and da/dt for the 2008 OS9 asteroid clones. The authors of the mentioned mercury software have published the first papers: Novakovic and Fenucci (2022) and Fenucci and Novakovic (2022).

As physical parameters in starting file yarkovsky.in, we used typical values of this type of asteroid, as was partially presented in Fenucci and Novakovic (2022):

- the density ρ (kg/m^3) = 2,120;
- the thermal conductivity K (W/m/K) = 0.001;
- the heat capacity C_h (J/kg/K) = 800;
- the diameter D (m) = 600;
- the obliquity γ (°) = for the first clone = 0, and of the following 100 clones differ from the previous one by $180/101°$ = 1.782 °;
- the rotation period P (h) = 8.43; taken from our previous work Cernis *et al.*, (2010)
- the absorption coefficient α; (usually set to 1);
- the emissivity ε (usually set to 1);

and as a starting parameter to the following files contained in the YORP file:

- yorp_flag = 1

i.e., include the spin-axis evolution due to the YORP effect;

- stoc_yorp_flag = 1

include stochastic YORP;

- step_user = 1.0

timestep for the spin-axis integration, *i.e.*, equal 1.0 year, *i.e.*, the minimum value for this integrator;

- dt_out = 1.0

timestep for printing output on a file;

- one year.

An assessment of the diameter of the asteroid Saule is in our previous article by Cernis *et al.*, (2010), where we used absolute magnitude H = 19.42 and different values of geometric albedo pV. The diameter of pV = 0.04 (C-type asteroid) is 867 m; for pV = 0.20 (S-type asteroid), it is 388 m. The true diameter of 2008 OS9 is between these two values.

In computations of the Yarkovsky and YORP effects, we accept the asteroid has a mean diameter of 600 m, and its mean albedo is 0.15. Hence, we take the mean diameter of the asteroid Saule in our computation.

We can check NEOWISE observations of NEOs for some infrared data on Saule. Sometimes, this can help in the determination of the geometric albedo. In our case,

Table 3: Starting nominal Keplerian orbital elements of the 428694 Saule (2008 OS9) asteroid

a (au)	*e*	*i* (°)	Ω (°)	*ω* (°)	*M* (°)
vfcc17 error model					
17 additional massive asteroids					
1.601243376	0.647927223	19.1403994	133.4127276	288.315140	200.179695
5.6×10^{-8}	7.4×10^{-8}	1.1×10^{-5}	8.8×10^{-6}	1.4×10^{-5}	3.4×10^{-5}

$H = 19.368$, RMSast = 0.367″, RMSmag = 0.427, $A_2 = (3.98 \pm 11.97) \times 10^{-14}$ au/d^2.
The angles ω, Ω, and i refer to Equinox J2000.0. Epoch: 2022 Jan 21=JD2459600.5 TDB.
H: absolute magnitude, RMSast: uncertainty of the fitted orbit, RMSmag: uncertainty of the absolute magnitude, A_2: non-gravitational transverse acceleration parameter.

we did not check NEOWISE data. We assume the albedo pV in the interval 0.05 ÷ 0.50, as is shown, for example, in Gustafsson *et al.*, (2019). Hence, we can compute the possible interval of the effective diameter of Saule: having both H and pV estimated as: $H = 19.39 \pm 0.5$ mag, pV = 0.27 ± 0.22 (both are systematic uncertainties, not standard deviations), one can proceed and estimate the effective diameter, D, which is $0.2 < D < 1$ km.

From a discussion above, it follows that the effective diameter of Saule can be determined only approximately. For this reason, we will do computations for a set of values presented in Table 4.

In turn, Table 4 indicates the calculation of the diameter of the asteroid Saule based on the range of observed H for 19.34, 19.39, and 19.44 mag and possible albedo, pV of 0.49, 0.27, and 0.05. For the diameters obtained in this way, we calculated the rotation periods of the asteroid for different bulk density densities of 1,000, 1,500, 2,000, and 2,500 kg/m^3 and for two mass cohesive trenches 10 and 100 Pa, respectively. We calculated the diameters of asteroid Saule according to the formula from Bowell *et al.*, (1978).

We then calculate the critical rotation period given by Hu *et al.*, (2021):

$$P_{\text{crit}} = 2\pi \sqrt{\frac{\rho k}{5C}}\, D, \tag{1}$$

where ρ is the bulk density, C is the bulk cohesion, and D is the diameter. According to Fenucci *et al.*, (2021), $k = 0.9114$ is a constant parameter, see Supplementary Material Pravec *et al.*, (2010).

Results are presented in Table 4. It turned out that the minimum periods of critical rotation are just over 2 h, for a density of 1,000 kg/m^3 and bulk cohesion 100 Pa, and maximum rotation periods of over 30 h occur for bulk density 2,500 kg/m^3 and bulk cohesion 10 Pa.

3.3 Long-time orbital and physical evolution

First, we computed orbital elements and non-gravitational elements of 101 clones of the asteroid 428694 Saule (2008 OS9) for epoch JD2459600.5 and the planets from Mercury

Table 4: Critical rotation periods for different starting physical parameters of the asteroid Saule

Absolute magnitude, H		19.34			19.39			19.44		
Visual albedo, pV		0.49	0.27	0.05	0.49	0.27	0.05	0.49	0.27	0.05
Diameter, D (m)		256	345	803	251	338	784	245	330	767
Density kg/m^3	**Bulk cohesion Pa**	**Critical rotation period**								
	Pa	**P_{crit}(h)**								
1,000	10	6.88	9.27	21.53	6.72	9.05	21.04	6.57	8.85	20.56
	100	2.17	2.93	6.81	2.13	2.86	6.65	2.08	2.80	6.50
1,500	10	8.42	11.35	26.37	8.23	11.09	25.77	8.04	10.84	25.18
	100	2.67	3.59	8.34	2.60	3.51	8.15	2.54	3.43	7.96
2,000	10	9.73	13.10	30.45	9.51	12.81	29.76	9.29	12.51	29.08
	100	3.08	4.14	9.63	3.00	4.05	9.41	2.94	3.96	9.20
2,500	10	10.87	14.65	34.04	10.63	14.32	33.27	10.39	13.99	32.51
	100	3.44	4.63	10.77	3.36	4.53	10.52	3.28	4.42	10.28

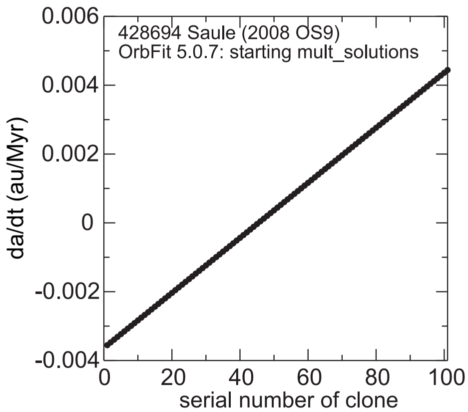

Figure 1: Starting non-gravitational parameter da/dt of 101 clones of the asteroid 428694 Saule (2008 OS9).

to Neptune. We used the parameter σLOV = 3 according to the multiple solution methods (Milani 2006, Milani *et al.*, 2005a, Milani *et al.*, 2005b), *i.e.*, the starting values of da/dt were obtained from the $A2$ parameter and its uncertainties.

Next, the starting orbital elements of each clone are treated as inputs in one small.in the file, and all of them, one yarkovsky.in a file is included, the same for all clones. These are the inputs to the main mercury integrator program. Of course, you can associate each clone's orbital elements with the same yarkovsky.in file. This way, we will have 101 input files with 101 data, yielding 101 × 101 calculation results. This would be a method close to a random method like the Monte Carlo method. However, this requires long, laborious calculations, and the line of variation (LOV) method of Milani avoids these difficulties. It does not require so many calculations.

Our additional computational tests showed that the computational results of one run of 101 clones yield similar to 101 × 101 computational results. So, the initial simplification of the number of integrations does not affect the result of calculations of the evolution of rotation, spin, and the non-gravitational parameter da/dt. Next, we integrated the equation of motions of asteroids and planets 0.5 Myr forward.

Figure 1 presents starting non-gravitational parameter da/dt of 101 clones of the asteroid 428694 Saule (2008 OS9) x computed from the OrbFit software. They are from (−0.004 to +0.006) au/Myr.

Figure 2 presents the physical parameters of asteroid 428694 Saule (2008 OS9) after 0.5 Myr forward integration. They are the rotation period P (h), the obliquity γ (°), and the value of da/dt connected with the non-gravitational

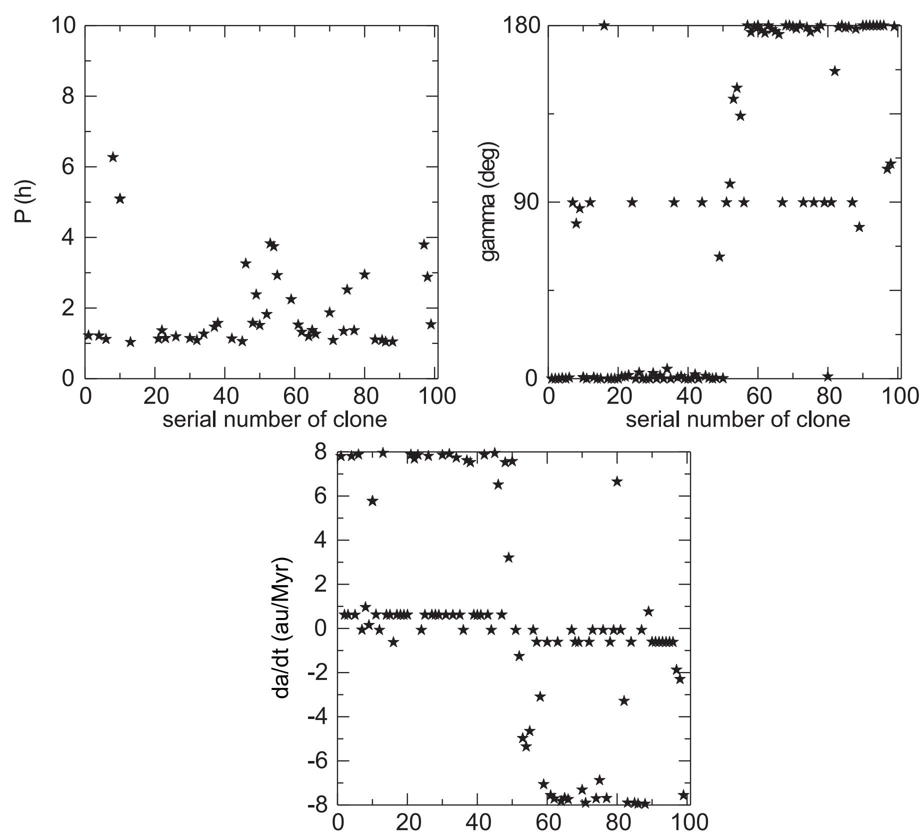

Figure 2: Physical parameters of asteroid 428694 Saule (2008 OS9) after 0.5 Myr forward integration. Parameter da/dt is multiplied by 10^4.

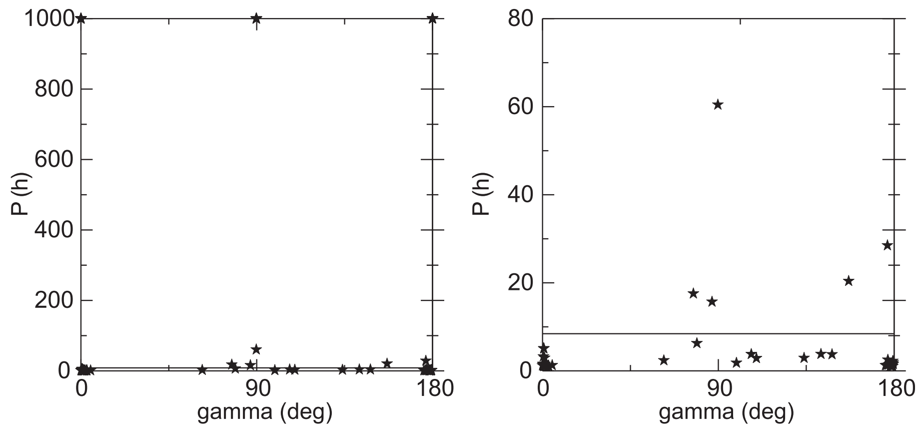

Figure 3: Left panel: Rotation period P vs spin axis of all clones of asteroid 428694 Saule (2008 OS9); 50 of them reached rotation period P = 1,000 h. Right panel: dependence of rotational period shorter than 80 h of 51 clones vs spin axis. Both panels present results of 0.5 Myr forward integration.

parameter $A2$. Only those clones with $P \leq 10$ h are marked in the left panel. There are 51 of them, so just over half. The other 50 have a rotation period, $P \geq 1{,}000$ h, and hence were assumed to have $P = 1{,}000$ h. According to the classification of the program, they slow down.

Hence, this state has a minor significance for the Yarkovsky effect, the semimajor axis drift $\mathrm{d}a/\mathrm{d}t$ goes to 0. We can see symmetry and possible correlation between spin axis gamma and non-gravitational parameter $\mathrm{d}a/\mathrm{d}t$ after 0.5 Myr forward integration. Those with gamma = 0° may give $\mathrm{d}a/\mathrm{d}t = 0$ or $\mathrm{d}a/\mathrm{d}t > 0$. In comparison, those with gamma = 180° may give $\mathrm{d}a/\mathrm{d}t$ negative or equal to 0. Hence, having the value of the gamma parameter, we can see something about the non-gravitational parameter $\mathrm{d}a/\mathrm{d}t$.

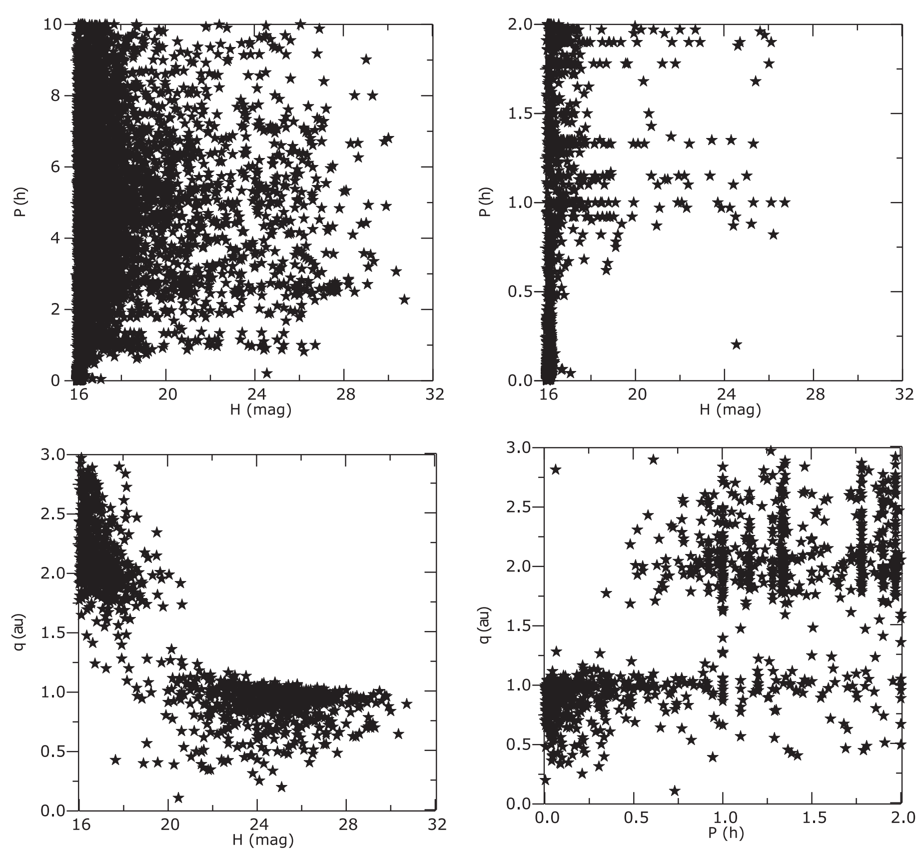

Figure 4: Known physical parameters of 31079 asteroids according to the MPC.

Comparing da/dt in Figure 2 (bottom panel), with da/dt from Figure 1, we can see that the amplitude of changes of the da/dt of the clones of the asteroid 428694 Saule (2008 OS9) after 0.5 Myr is about 20 times smaller than the starting one, that is, from a range of about ±0.004 au/Myr to about ±0.0008 au/Myr.

It is interesting that after a period of 0.5 Myr, the clones' da/dt values are around the borderline values −0.0008 au/Myr and +0.0008 au/Myr, and also around da/dt = 0.

Hence, the dynamics of changes in the da/dt value decreases, and the clones seem to slow down, stay close to a particular achieved place, and move slower in both directions of their semimajor axis. The second part of the clones is around the value da/dt = 0 au/Myr, meaning that they practically do not change their positions on the semimajor axis related to the Yarkovsky effect. Such stratification of clones on the da/dt axis begins to appear after about 100,000 years and is visible after 0.5 Myr.

Interesting is the distribution of the clonal rotation period. As shown in the left panel of Figure 2, the rotation period of the clones P is generally between 1 and 2 h, from the original value P, of 8.43 h. So, the asteroid clones sped up their rotation period by almost nine times.

Given the diameter of the asteroid Saule (D = 600 m) and its assumed density of 2,120 kg/m^3, the asteroid is most likely a rubble pile held by gravity forces. The shortest rotation period for such objects is P = 2.1 h, at which they experience resurfacing (*e.g.*, creation of a typical top-hat shape), mass shading, or even rotational fission into several smaller objects. This fact has been considered by Fenucci and Novakovic (2022), who set a limit at some critical period P_{crit} = 2.34 h for his asteroid with a diameter of 2 km.

They write: "When the rotation period becomes smaller than P_{crit} we assume that a fission event takes place and we re-initialize the spin state. In this process, we do not simulate production of a binary system, and we assume that the mass lost is small enough to not significantly change the equivalent diameter of the object. During the fission event, we assume the obliquity *gamma* to be unchanged. On the other hand, the spin rate is decreased according to the momentum carried away by the ejected mass." As a result, the rotation period is never smaller than P_{crit}. Note that during test runs of the Mercury N-body code, periods were never smaller than this critical value, see Figure 4 in Fenucci and Novakovic (2022).

Table 5: Number of clones in a given state for K = 0.001

Time	10 ky	100 ky	500 ky
	Number of clones		
P (h)			
1,000	0	25	50
1–10	99	55	51
Others	2	21	0
Gamma (°)			
0	1	8	23
90	4	6	13
180	1	13	32
Others	95	74	31
da/dt (au/day^2)			
<0	51	51	53
>0	50	50	48

Table 6: Number of clones with P = 10,000 h in a given state of spin axis after 0.5 Myr forward integration

Spin axis (°)	Number of clones (% of all starting clones)
0	22 (21.8)
90	13 (12.9)
180	15 (14.9)

Similarly interesting is the distribution in the inclination of the rotation axis of the clones to the ecliptic plane. Initially, we assumed that the neighboring clones differ by 180/101° in the gamma angle, *i.e.*, in the inclination of the rotation axis. There is a visible polarization to 0, 90, and 180°.

Hence, our computations showed that the Yarkovsky effect plays a significant role after 0.5 Myr, and even signs of it are already visible after 0.1 Myr.

Figure 3 presents the rotation period P vs. spin axis of all clones of asteroid 428694 Saule (2008 OS9), 50 reached rotation period P = 10,000 h (left panel) and dependence of rotational period shorter than 80 h of 51 clones vs. spin axis (right panel). Both panels present results of 0.5 Myr

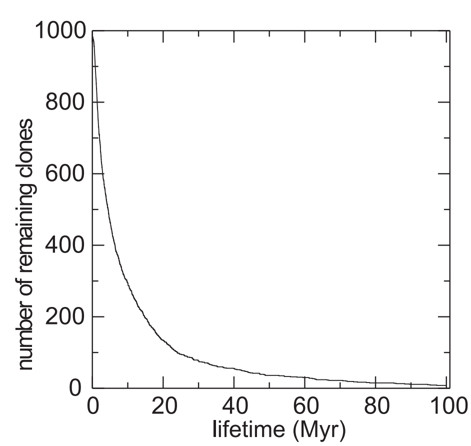

Figure 5: The Centaur 2009 HW77. The behavior of the lifetime of the remaining clones has an exponential shape. Hence we can compute the half-time of 1,001 clones in the forward 100 Myr RA15 integration. The computed half-time is 4.45 Myr.

Table 7: Initial nominal Keplerian orbital elements of the 330836 Orius (2009 HW77) asteroid

a (au)	e	i (°)	Ω (°)	ω (°)	M (°)
vfcc17 error model					
17 Additional massive asteroids					
21.502244	0.4169934	17.8749641	50.451470	141.037047	54.14741
7.13×10^{-4}	1.76×10^{-5}	3.47×10^{-5}	6.26×10^{-5}	3.15×10^{-4}	2.78×10^{-3}

H = 9.749, RMSast = 0.519, RMSmag = 0.352.
The angles ω, Ω, and i refer to Equinox J2000.0. Epoch: 2022 Jan 21 = JD2459600.5 TDB.

forward integration. It is visible that clone groups near 0, 90, and 180°. In particular, this is visible in the case of clones that have reached their period's rotation equal to 1,000 h.

Table 5 shows the number of the first group of clones for the three spin-axis groups. It turned out that they take only three spin-axis values: 0, 90, and 180° (Table 6).

3.4 Known rotation periods of asteroids

According to the recent reliable database of the asteroid rotation periods: https://minplanobs.org/mpinfo/datazips/LCLIST_PUB_2023JUN.zipthere are 32778 asteroids with defined physical parameters.

According to the database, they introduce the U code, which assesses the quality of the period solution, not necessarily of the data per se, as stated there.

If we selected asteroids with criterion $U \geq -2$, we got 31,079 asteroids. Figure 4 presents their rotational period vs. diameter. For visibility, only every fifth asteroid is presented.

Additionally, if we count objects which fulfill the following criteria:

H: <20 mag,

P: <2 h we got only a few selected asteroids. Hence, the asteroid 2008 OS9, NEA, with starting q = 0.5 au, may have during his evolution the theoretical rotation period around 1 h as we computed using the mercury software.

4 Orbital evolution of the asteroid 330836 Orius (2009 HW77)

The centaur Orius, who lived in the mountains, was killed by Heracles when he tried to steal the wine Pholus.

4.1 Starting orbital elements

KC and IE discovered Asteroid 330836 Orius (2009 HW77) at Baldone on 2009-04-25. An orbit type of asteroid is a Distant object. To compute starting orbital elements of the asteroid Orius, we used the OrbFit software with the JPL DE431 ephemerides, weighting and selecting observations according to the (NEODyS-2)[3], 17 additional massive asteroids. We did not search for the non-gravitational parameter $A2$ because of the long distance of the asteroid to the Sun and the high absolute magnitude of the asteroid. We used all 85 observations published by the IAU MPC from 2002 02 12.50951 to 2012 05 19.44276.

According to the OrbFit v5.0.7, we used the error model *vfcc17* (Veres *et al.*, 2017). Table 5 presents the initial nominal Keplerian orbital elements of the 330836 Orius (2009 HW77) asteroid.

4.2 Long-time orbital evolution

The dynamical lifetime is the time between the start of integration and ejection from the integration. The studied asteroid 330836 Orius (2009 HW77), like other Centaurs, are planet-crossing object and has relatively short dynamical lifetimes of around 1 Myr (Horner *et al.*, 2004) and short Lyapunov time, *e.g.*, of about 4,260 year for Centaur asteroid (463,368) 2012 VU12 (Wlodarczyk *et al.*, 2017).

Due to the lack of sufficiently precise physical parameters of the asteroid 2009 HW77, to study its orbital evolution we used SWIFT software, initially developed by H. Levison (https://www.boulder.swri.edu/~hal/swift.html).

We included perturbations of all planets from Mercury to Neptune. We computed clones using the multiple solution methods for the 1σ uncertainty around the nominal orbit of the asteroid. We computed the time evolution of all 1,001 starting clones during 100 Myr of forward integration. The integration is similar to that of Wlodarczyk *et al.*, (2011). Clones that reached the ejection distance (1,000 au) or that impacted the Sun or a planet were removed from our integration. The computed half-time,

3 https://newton.spacedys.com/neodys/

Table 8: Starting nominal Keplerian orbital elements of the 2017 UW42 asteroid

a (au)	e	i (°)	Ω (°)	ω (°)	M (°)
vfcc17 error model					
17 additional massive asteroids					
2.4556296374	0.4843383688	6.67099688	287.45079556	195.52571430	99.31791520
2.394×10^{-7}	8.74×10^{-8}	5.28×10^{-6}	2.936×10^{-5}	4.233×10^{-5}	1.828×10^{-5}

H = 17.938, RMSast = 0.4418, RMSmag = 0.346, $A_2 = (1.24 \pm 1.66) \times 10^{-12}$ au/day^2.
The angles ω, Ω, and i refer to Equinox J2000.0. Epoch: 2023 Feb. 25 = JD2460000.5 TDB.

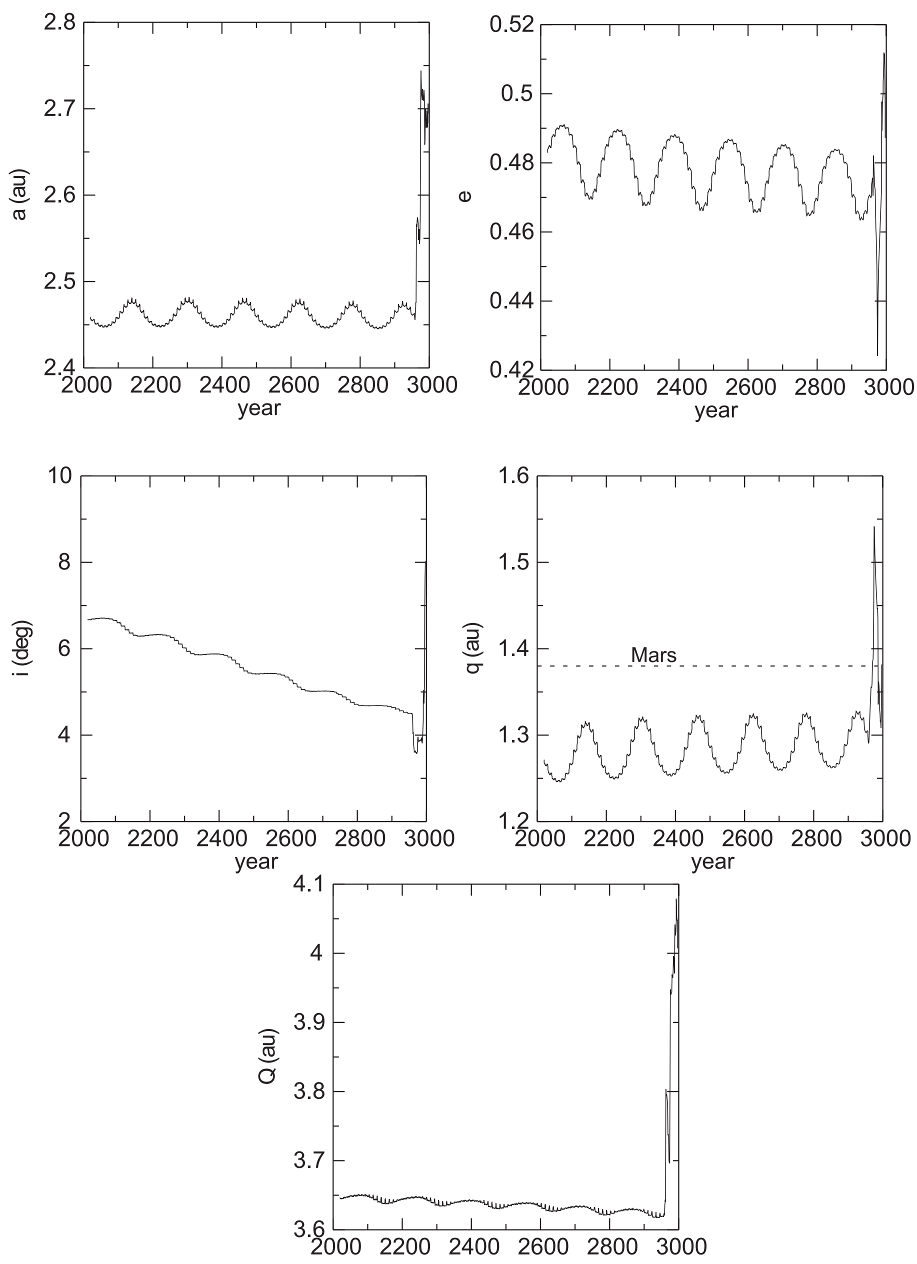

Figure 6: Asteroid 2017 UW42. The orbital evolution of the semimajor axis, eccentricity, inclination, perihelion distance, and aphelion distance of the asteroid 2017 UW42.

i.e., when half of the clones are rejected, is 4.45 Myr, as shown in Figure 5. Wlodarczyk *et al.*, (2011) computed a half-time of 5.25 Myr in our previous paper. The differences result from a more accurate orbit based on a longer observation arc. Also, previously starting orbital elements of the asteroid are computed only with added Ceres, Pallas, and Vesta, now 17 additional massive asteroids.

5 Keplerian orbital elements of the asteroid 2017 UW42

It is also worth paying attention to the interesting asteroid 2017 UW42. According to the MPC site: https://minorplanetcenter.net/iau/mpc.htmlasteroid 2017 UW42 was first observed at Mt. Lemmon Survey on 2017-10-27. It was independently discovered by (KC, IE) on Sep. 26, 2017. Discoverer will be defined when the object is numbered. Table 7 presents initial nominal Keplerian orbital elements of the 330836 Orius (2009 HW77) asteroid. Interestingly, that studied asteroid has a significant value of the non-gravitational parameter A_2 = (1.24 ± 1.66) × 10^{-12} au/day^2 in comparison with other asteroids, see *e.g.*, Figure 2, left panel in Wlodarczyk (2022). Table 8 presents starting nominal Keplerian orbital elements of the 2017 UW42 asteroid.

Figure 6 presents the orbital evolution of semimajor axis, eccentricity, inclination, perihelion distance, and aphelion distance of the asteroid 2017 UW42.

All orbital computations and analyses of results, including Figures 1, 2, 3, 4, 5, 6 using different software presented in this work was made by one of us (IW).

6 Summary

We discovered 83 asteroids at the Baldone Astrophysical Observatory (MPC 069) in 2017–2022. We studied one of the dynamically interesting Apollo (NEO) observed at the Baldone Astronomical Observatory, namely 428694 Saule (2008 OS9) and the Centaur-type asteroid 330836 Orius (2009 HW77). Additionally, we studied the orbit of the Amor-type asteroid 2017 UW42 with the significant non-gravitational parameter $A2$.

Acknowledgement: We want to thank the anonymous reviewers for their many helpful suggestions. IW thanks the Space Research Center of the Polish Academy of Sciences in Warsaw for the chance to work on a computer cluster. Our thanks go to the ERDF Project No. 1.1.1.5/19/A/003.

Funding information: This work has been supported by the ERDF project No. 1.1.1.5/19/A/003 made by KC and IE.

Author contributions: All authors have accepted responsibility for the entire content of this manuscript and consented to its submission to the journal, reviewing all the results and approving the final version of the manuscript. KC and IE discovered all asteroids, and KC made Tables 1 and 2 with discoveries. IW developed the model code and performed the simulations. IW prepared the manuscript in Latex with contributions from all co-authors.

Conflict of interest: The authors state no conflict of interest.

Data availability statement: All starting data of orbital elements and the source code of the OrbFit software were accessed from: https://ssd.jpl.nasa.gov/tools/sbdb_lookup.html#/, https://minorplanetcenter.net/db_search and https://newton.spacedys.com/astdys/.

References

Bowell E, Chapman CR, Gradie JC, Morrison D, Zellner B. 1978. Taxonomy of asteroids. Icarus. 35:313–335. doi: https://doi.org/10.1016/0019-1035(78)90085-4.

Chambers JE 1999. A hybrid symplectic integrator that permits close encounters between massive bodies. Monthly Notices R Astron Soc. 304:793–799. doi: https://doi.org/10.1046/j.1365-8711.1999.02379.x.

Černis K, Eglitis I, Wlodarczyk I, Zdanavičius J, Zdanavičius K. 2010. The Apollo group asteroid 2008 OS9: Discovery, orbit, rotation and the Yarkovsky/YORP effects. Baltic Astron. 19:235–263. doi: https://doi.org/10.1515/astro-2017-0424.

Černis K, Wlodarczyk I, Eglitis I. 2015. Observational data and orbits of the asteroids discovered at the Baldone Observatory in 2008–2013. Baltic Astron. 24:251–262. doi: https://doi.org/10.1515/astro-2017-0226.

Dziadura K, Spoto F, Oszkiewicz D, Carry B, Bartczak P, Tanga P. 2022. Computing the Yarkovsky effect for asteroids in Gaia DR3. European Planetary Science Congress. doi: https://doi.org/10.5194/epsc2022-649.

Farnocchia D, Chesley SR, Vokrouhlický D, Milani A, Spoto F, Bottke WF. 2013a. Near Earth asteroids with measurable Yarkovsky effect. Icarus. 224:1–13. doi: https://doi.org/10.1016/j.icarus.2013.02.004.

Farnocchia D, Chesley SR, Chodas PW, Micheli M, Tholen DJ, Milani A, et al. 2013b. Yarkovsky-driven impact risk analysis for asteroid (99942) Apophis. Icarus 224:192–200. doi: https://doi.org/10.1016/j.icarus.2013.02.020.

Fenucci M, Novaković B. 2022. MERCURY and ORBFIT packages for numerical integration of planetary systems: Implementation of the Yarkovsky and YORP effects. Serbian Astron J. 204:51–63. doi: https://doi.org/10.2298/SAJ2204051F.

Fenucci M, Novaković B, Vokrouhlický D, Weryk RJ. 2021. Low thermal conductivity of the superfast rotator (499998) 2011 PT. Astron Astrophys. 647:A61. doi: https://doi.org/10.1051/0004-6361/202039628.

Gustafsson A, Trilling DE, Mommert M, McNeill A, Hora JL, Smith HA, et al. 2019. Spitzer albedos of near-Earth objects. Astron J. 158:67. doi: https://doi.org/10.3847/1538-3881/ab29ea.
Horner J, Evans NW, Bailey ME. 2004. Simulations of the population of Centaurs - I. The bulk statistics. Monthly Notices R Astron Soc. 354:798–810. doi: https://doi.org/10.1111/j.1365-2966.2004.08240.x.
Hu S, Richardson DC, Zhang Y, Ji J. 2021. Critical spin periods of sub-km-sized cohesive rubble-pile asteroids: dependences on material parameters. Monthly Notices R Astronom Soc. 502:5277–5291. doi: https://doi.org/10.1093/mnras/stab412.
Milani A 2006. Asteroid impact monitoring. Serbian Astronom J. 172:1–11. doi: https://doi.org/10.2298/SAJ0672001M.
Milani A, Chesley SR, Sansaturio ME, Tommei G, Valsecchi GB. 2005a. Nonlinear impact monitoring: line of variation searches for impactors. Icarus 173:362–384. doi: https://doi.org/10.1016/j.icarus.2004.09.002.
Milani A, Sansaturio ME, Tommei G, Arratia O, Chesley SR. 2005b. Multiple solutions for asteroid orbits: Computational procedure and applications. Astron Astrophys. 431:729–746. doi: https://doi.org/10.1051/0004-6361:20041737.
Novakovic B, Fenucci M. 2022. Mercury and OrbFit packages for numerical orbit propagation: Implementation of the Yarkovsky and YORP effects. 16th Europlanet Science Congress. Spain: Palacio de Congresos de Granada.
Novaković B, Vokrouhlický D, Spoto F, Nesvorn&#1acute; D 2022. Asteroid families: properties, recent advances, and future opportunities. Celestial Mech Dyn Astron. 134:34. doi: https://doi.org/10.1007/s10569-022-10091-7.
Perez-Hernandez J, Benet L. 2022. Non-zero Yarkovsky acceleration for near-Earth asteroid (99942) Apophis. AAS/Division Dynam Astron Meeting.
Pravec P, Vokrouhlický D, Polishook D, Scheeres DJ, Harris AW, Galad A, et al. 2010. Formation of asteroid pairs by rotational fission. Nature 466:1085–1088. doi: https://doi.org/10.1038/nature09315.
Vereš P, Farnocchia D, Chesley SR, Chamberlin AB. 2017. Statistical analysis of astrometric errors for the most productive asteroid surveys. Icarus. 296:139–149. doi: https://doi.org/10.1016/j.icarus.2017.05.021.
Wlodarczyk I, Cernis K, Eglitis I. 2011. Analysis of the orbit of the Centaur asteroid 2009 HW77. Monthly Notices R Astronom Soc 418:2330–2335. doi: https://doi.org/10.1111/j.1365-2966.2011.19621.x.
Wlodarczyk I 2015. The Potentially Hazardous Asteroid (410777) 2009 FD. Acta Astronom. 65:215–231.
Wlodarczyk I, Černis K, Boyle RP. 2017. Discovery, orbit and orbital evolution of the distant object (463368) 2012 VU85. Acta Astronom. 67:81. doi: https://doi.org/10.32023/0001-5237/67.1.6.
Włodarczyk I. 2018. Non-gravitational parameters in motion of asteroid. XXXVIII Polish Astron Soc Meet. 7:141–143.
Wlodarczyk I, Leliwa-Kopystynski J 2018. Forward orbital evolution of the Vesta Family with and without the Yarkovsky effect. Bulgarian Astron J. 28:79.
Wlodarczyk I. 2020. Bulgarian Astron J. 32:27.
Wlodarczyk I, Cernis K, Boyle RP. 2022a. Observational data and orbits of the asteroids discovered at the VATT Observatory in 2010–2012. Bulgarian Astron J. 2022;37:31.
Wlodarczyk I. 2022b. Non-gravitational parameters and orbital stability of asteroids in retrograde orbits. Monthly Notices R Astronom Soc. 516:6116–6122. doi: https://doi.org/10.1093/mnras/stac2603.